Biomedical Signal Processing and Control 66 (2021) 102421

Contents lists available at ScienceDirect

Biomedical Signal Processing and Control

journal homepage: www.elsevier.com/locate/bspc

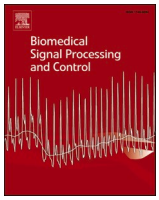

Modeling of artifacts in the wrist photoplethysmogram: Application to the detection of life-threatening arrhythmias

Birutė Paliakaitė [a,*], Andrius Petrėnas [a], Andrius Sološenko [a], Vaidotas Marozas [a,b]

[a] Biomedical Engineering Institute, Kaunas University of Technology, 51423 Kaunas, Lithuania
[b] Department of Electronics Engineering, Kaunas University of Technology, 51368 Kaunas, Lithuania

ARTICLE INFO

Keywords:
Motion artifacts
Artifact characterization
Signal quality index (SQI)
Wearable device
Bradycardia
Tachycardia

ABSTRACT

Objective: A model for simulating motion-induced artifacts in the wrist photoplethysmogram (PPG) is proposed for the purpose to improve realism of PPG models.
Methods: The database of day-long PPGs, acquired during cardiac rehabilitation, is used to extract artifact characteristics, which further serve as a basis for modeling artifacts in simulated PPGs with life-threatening arrhythmias.
Results: Depending on the recording, 14–49% of the PPG duration is corrupted by artifacts, mostly due to device displacement, forearm and hand motion. The artifact type influence on the performance of a life-threatening arrhythmia detector shows that the sensitivity drops by 45–48% for extreme bradycardia and by 13–32% for ventricular tachycardia. Poor contact causes 2–4 times more false alarms of ventricular tachycardia compared to the other artifact types under investigation.
Conclusion: Simulation of realistic artifacts encountered in activities of daily living allows to comprehensively investigate arrhythmia detectors and understand the artifact types most negatively affecting detection performance.
Significance: The proposed PPG artifact model is of importance for developing and testing artifact-robust arrhythmia detectors.

1. Introduction

Sudden cardiac death accounts for 15–20% of all deaths [1]. In general, ventricular tachycardia, evolving to ventricular fibrillation, often precedes sudden cardiac death [2]. Also, a recent research shows that extreme bradycardia can be a common cause in certain populations, e.g., in patients with chronic kidney disease [3]. Patients at risk of sudden cardiac death due to life-threatening arrhythmias could potentially benefit from implantation of a cardiac pacemaker or a cardioverter defibrillator [4]. However, to initiate a proper treatment and careful supervision of these patients, monitoring for the detection of initial arrhythmia episodes is needed.

The existing electrocardiogram (ECG) equipment for noninvasive arrhythmia monitoring is uncomfortable to wear for extended periods of time because of frequent skin irritation, difficulty of use, and disturbance to patient's daily activities [5]. Even ECG patch monitors, praised for high patient compliance, are limited to 14-day recording [6]. Therefore, smartwatches with embedded optical sensors are being considered as convenient means to initial cardiac arrhythmia detection, which may precede and instigate comprehensive medical examination and timely clinical intervention [7,8]. Recently, detection of atrial fibrillation in a photoplethysmogram (PPG) has demonstrated encouraging results and received wide-scale research attention [9–13]. Likely, the tremendous potential of smartwatches capable of detecting atrial fibrillation will spawn the development of other type arrhythmia detectors. However, thus far only a single attempt to detect life-threatening arrhythmias in a PPG has been published [14].

Susceptibility to artifacts hinders the application of a wrist PPG in activities of daily living since artifacts often result in missed arrhythmia episodes and false alarms. Efforts have been made to reduce motion artifacts using accelerometer and gyroscope signals [15–21], whereas finer hand motions, which do not reflect in biomechanical data, can be dealt by using different PPG wavelengths and a piezoelectric transducer [22–24]. Signal processing techniques have also been invoked for PPG quality estimation [25] and motion artifact reduction [26]. Yet, none of these approaches to artifact suppression have been applied for cardiac

* Corresponding author.
E-mail address: birute.paliakaite@ktu.lt (B. Paliakaitė).

https://doi.org/10.1016/j.bspc.2021.102421
Received 25 August 2020; Received in revised form 26 October 2020; Accepted 10 January 2021
Available online 2 February 2021

arrhythmia detection.

A common way to deal with artifact-corrupted PPGs, and thus improve the reliability of arrhythmia detectors, is to exclude segments of poor signal quality [10,27,28] as well as accelerometer-identified motion [11–13,27–30]. Although segment removal conceals the true detection performance, it is not a major problem in case of atrial fibrillation which often lasts for hours without being dangerous [31]. In contrast, even short episodes of extreme bradycardia and ventricular tachycardia can be life-threatening requiring immediate intervention. Moreover, identification of target patients for collection of signal databases is markedly facilitated when dealing with an often long-lasting arrhythmia, such as atrial fibrillation, thus making detector development and validation less complicated.

Detectors are usually tested in a controlled environment, thus offering incomplete insight into the feasibility to detect arrhythmias in free-living activities [32]. Accordingly, such algorithms cannot claim robustness without considering artifact influence on the performance. However, to analyze the detector performance in long-term PPGs, arrhythmias must be annotated, which is time-consuming and costly. Another impeding factor is that annotations must rely on a simultaneously acquired ECG due to the absence of guidelines for a PPG-based arrhythmia diagnosis. Apparently, all these restrictions have a large impact on the lack of available databases, containing PPGs with annotated arrhythmia episodes. The problem can be mitigated by developing and testing arrhythmia detectors on modeled PPGs, thanks to the available model that allows to convert annotated ECG databases to PPG equivalents [33,34]. Unfortunately, only a stationary artifact component can be simulated by the model without considering various artifact types which may have different influence on the detection performance.

To build a realistic PPG artifact model, quantitative characteristics, such as artifact duration, amplitude, and spectral content, have to be accounted for [35,36]. In this study, different-type artifacts are quantitatively assessed from ambulatory PPGs and their characteristics are invoked to develop an artifact model.[1] The paper is organized as follows. Section 2 describes artifact identification, extraction, classification, and characterization. Section 3 introduces artifact modeling. Section 4 describes databases used for model development and for testing a life-threatening arrhythmia detector. Section 5 presents the quantitative artifact analysis as well as the results on the model application to testing detector performance. The paper finishes with a discussion of the results.

2. Artifact analysis

Artifact analysis is implemented in four steps: identification, extraction, classification, and characterization, see Fig. 1. Artifact-corrupted PPG segments are identified relying on a signal quality index (SQI) proposed in [10]. Then, the artifacts are extracted by canceling the modeled pulsatile PPG component, and classified into four types characterized by a transition probability, an artifact duration, a spectral slope, and a normalized root mean square (RMS) amplitude.

2.1. Artifact identification

Artifacts in a PPG are identified using an SQI on a pulse-to-pulse basis [10]. Before applying the SQI, the PPG is filtered with a low-pass infinite impulse response filter with a cut-off frequency of 6 Hz. Baseline wander is removed using a fifth-order least mean squares adaptive filter. The occurrence times of the PPG pulses are determined using a peak detector similar to the one described in [37].

The signal quality of the kth pulse $x_k(n)$, $k = 1, \ldots$, is assessed by correlating it to a template pulse $g_k(n)$ at different time shifts θ_k, using the sample correlation coefficient. Before correlating, $x_k(n)$ and $g_k(n)$ are standardized, and $g_k(n)$ is resampled to the width of $x_k(n)$. The signal quality is considered acceptable when the maximum correlation coefficient $\widehat{c}_{max,k}$ exceeds the threshold η_c, i.e., the binary SQI s_k is defined by

$$s_k = \begin{cases} 1, & \widehat{c}_{max,k} \geq \eta_c, \\ 0, & \text{otherwise}. \end{cases} \tag{1}$$

The initial template pulse $g_1(n)$ is a predefined PPG pulse $h(n)$ with a dicrotic notch [38]. The subsequent templates $g_{k+1}(n)$ are determined by the preceding pulse $x_k(n)$ if $\widehat{c}_{max,k}$ exceeds the threshold ξ_c and $\widehat{\theta}_k$ is contained in the time interval $[\theta_{min}, \theta_{max}]$; if not, $g_{k+1}(n)$ is reinitialized by $h(n)$, i.e.,

$$g_{k+1}(n) = \begin{cases} x_k(n), & \widehat{c}_{max,k} \geq \xi_c \ \ \& \ \ \widehat{\theta}_k \in [\theta_{min}, \theta_{max}], \\ h(n), & \text{otherwise}, \end{cases} \tag{2}$$

where ξ_c is set to 0.95 and $[\theta_{min}, \theta_{max}]$ are set to $[-0.05, 0.05]$ s. The threshold η_c is set to 0.7 based on the findings of the previous study, in which the PPG pulses with maximum correlation coefficient $\widehat{c}_{max,k}$ below 0.7 were considered to be of poor quality [10].

By inspecting PPGs acquired in free-living activities, high-amplitude artifacts similar to PPG pulses, which exceed the threshold $\eta_c = 0.7$, have been observed. Taking this into account, pulses with a peak-to-peak amplitude higher than 95th percentile of all pulses in the entire recording, also satisfying $\widehat{c}_{max,k} < 0.9$, are considered of poor quality. Adjacent poor-quality pulses, as well as those separated by a single good-quality pulse, are assumed to constitute a single continuous artifact-corrupted PPG segment.

2.2. Artifact extraction

An unprocessed PPG is a subject to artifact extraction, only with a slow-changing component below 0.5 Hz eliminated. Then, it is assumed that the remaining PPG consists of heart contraction-related pulsations and artifacts. An artifact-free pulsatile component is generated using a PPG simulation model described in [33,34], which uses RR intervals of the synchronously acquired ECG as an input. The lth artifact $\nu_l(n)$, $l = 1, \ldots$, is extracted by canceling the modeled component from the PPG using a least-mean squares adaptive filter. It should be noted that artifacts cannot be extracted when ECG of sufficient quality for obtaining RR intervals is unavailable.

2.3. Artifact classification

The extracted artifacts are classified into four types: device displacement, forearm motion, hand motion, and poor contact (Fig. 2). The classification of the lth artifact $\nu_l(n)$ is based on three features obtained from a synchronously acquired accelerometer signal and the artifact itself.

The mean absolute acceleration u_l, quantified from the accelerometer signal, is used to identify device displacement and forearm motion, and is defined by

$$u_l = \frac{1}{N_l} \sum_{n=1}^{N_l} \left(|a_x(n)| + |a_y(n)| + |a_z(n)| \right), \tag{3}$$

where N_l determines the number of samples in the lth artifact, whereas a_x, a_y, a_z represent a high-pass filtered accelerometer signal in g units from x, y, and z directions.

The adjusted amplitude v_l represents the largest amplitude difference within the artifact, and is defined by

$$v_l = \frac{max_{1<n<N_l} \nu_l(n) - min_{1<n<N_l} \nu_l(n)}{\text{iqr}_\nu}, \tag{4}$$

where iqr_ν is the interquartile range of amplitude values in all extracted artifacts over the entire recording.

[1] Note: the code for test signal generation will be made available at PhysioNet upon manuscript publication.

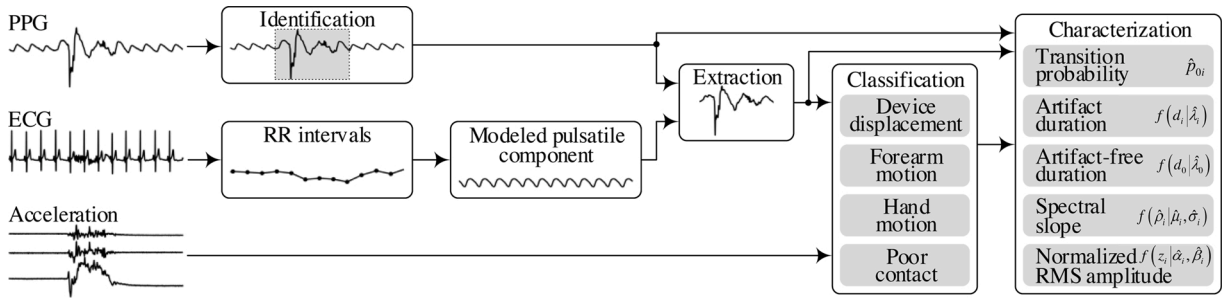

Fig. 1. Block diagram of artifact analysis consisting of artifact identification, extraction, classification, and characterization.

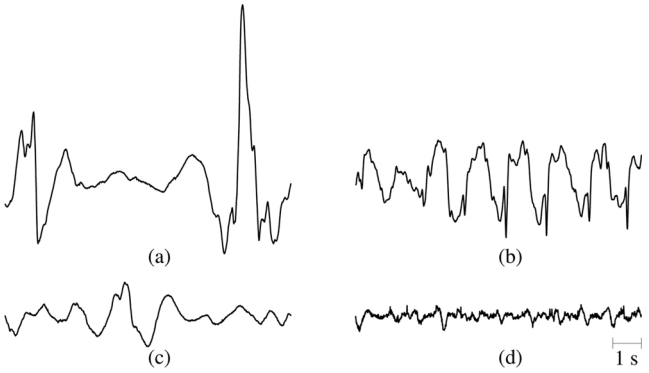

Fig. 2. Examples of common artifacts encountered in the wrist PPG: (a) device displacement, (b) forearm motion, (c) hand motion, and (d) poor contact. The modeled pulsatile PPG component is canceled.

The spectral flatness w_l expresses the resemblance of artifact spectral properties to those of white noise, and is calculated as a ratio between geometric and arithmetic means of the power spectral density (PSD) of the extracted artifact

$$w_l = \frac{exp\left(\frac{1}{M}\sum_{m=0}^{M-1} ln\widehat{P}_l(m)\right)}{\frac{1}{M}\sum_{m=0}^{M-1}\widehat{P}_l(m)}, \tag{5}$$

where $\widehat{P}_l(m)$ is a non-parametric PSD estimate at each frequency bin m, and M is the number of frequency bins.

Artifacts are classified by comparing u_l, v_l, and w_l with the predefined thresholds η_u, η_v, and η_w. The type of the artifact $\nu_l(n)$ is determined according to the following rules:

$$\begin{aligned}
&\text{device displacement,} && \text{if } u_l > \eta_u \ \&\ v_l > \eta_v,\\
&\text{forearm motion,} && \text{if } u_l > \eta_u \ \&\ v_l \le \eta_v,\\
&\text{hand motion,} && \text{if } u_l \le \eta_u \ \&\ w_l \le \eta_w,\\
&\text{poor contact,} && \text{if } u_l \le \eta_u \ \&\ w_l > \eta_w.
\end{aligned}$$

Given that even very brief artifacts, lasting just few seconds, are also likely, the minimal artifact duration d_{min} has to be determined to increase feature robustness.

2.4. Artifact characterization

The transition probability p_{0i} from an artifact-free interval to an artifact is estimated as

$$\widehat{p}_{0i} = \frac{R_i}{\sum_{i=1}^{4} R_i}, \tag{6}$$

where R_i is the number of artifacts classified as a type i. The index i equal to 1 indicates device displacement, 2 – forearm motion, 3 – hand motion, and 4 – poor contact.

The duration d_i of the extracted artifacts can be described by an exponential distribution

$$f(d_i|\lambda_i) = \begin{cases} \lambda_i e^{-\lambda_i d_i}, & d_i \ge 0,\\ 0, & d_i < 0, \end{cases} \tag{7}$$

where λ_i is the rate parameter equal to the reciprocal of the mean. An estimate of the rate parameter $\widehat{\lambda}_i$ is obtained using maximum likelihood estimation. The duration of artifact-free intervals is described in the same way with an estimate of the rate parameter denoted by $\widehat{\lambda}_0$.

The spectral slope ρ_i, which depends on artifact spectral characteristics, is estimated from the average PSD calculated as

$$\overline{P}_i(m) = \frac{10\sum_{r_i=1}^{R_i} N_{r_i} log_{10}\widehat{P}_{r_i}(m)}{\sum_{r_i=1}^{R_i} N_{r_i}}, \tag{8}$$

where $\widehat{P}_{r_i}(m)$ is a non-parametric PSD estimate of the rth standardized artifact of a type i, whereas N_{r_i} is the number of samples in the artifact. Then, the spectral slope $\widehat{\rho}_i$ is estimated in each recording by fitting a line to $\overline{P}_i(m)$ within a frequency range from 0.5 to 50 Hz. The spectral slope $\widehat{\rho}_i$ can be described by a Gaussian distribution with mean $\widehat{\mu}_i$ and standard deviation $\widehat{\sigma}_i$.

The normalized RMS amplitude z_i of the type i artifact is estimated in 1-s segments as the RMS of the extracted artifact normalized by the RMS of the pulsatile component at the output of the adaptive filter described in Section 2.2. The normalized RMS amplitude z_i can be described by a gamma distribution with estimated shape $\widehat{\alpha}_i$ and rate $\widehat{\beta}_i$ parameters.

3. Artifact modeling

The transitions between artifact-free intervals and artifacts are modeled by a five-state continuous-time Markov chain, where the state 0 represents an artifact-free interval and the states from 1 to 4 correspond to ith-type artifacts. The transition from the artifact-free interval to all four artifact types is possible; however, only the transition to the artifact-free interval is allowed from the artifact. The generator matrix of the described Markov process is defined by

$$Q = \begin{bmatrix} -\lambda_0 & \lambda_0 p_{01} & \lambda_0 p_{02} & \lambda_0 p_{03} & \lambda_0 p_{04}\\ \lambda_1 & -\lambda_1 & 0 & 0 & 0\\ \lambda_2 & 0 & -\lambda_2 & 0 & 0\\ \lambda_3 & 0 & 0 & -\lambda_3 & 0\\ \lambda_4 & 0 & 0 & 0 & -\lambda_4 \end{bmatrix} \tag{9}$$

The type i artifact is generated by filtering white noise with a 250th order finite impulse response filter designed so that its arbitrary shape frequency response is determined by the spectral slope taken from the Gaussian distribution with the parameters $\widehat{\mu}_i$ and $\widehat{\sigma}_i$. The amplitude of the generated artifact is scaled by the normalized RMS amplitude taken from the gamma distribution with the parameters $\widehat{\alpha}_i$ and $\widehat{\beta}_i$. Finally, the connected signal of artifacts and artifact-free intervals is added to the modeled pulsatile component to produce a PPG with life-threatening arrhythmias and artifacts as shown Fig. 3.

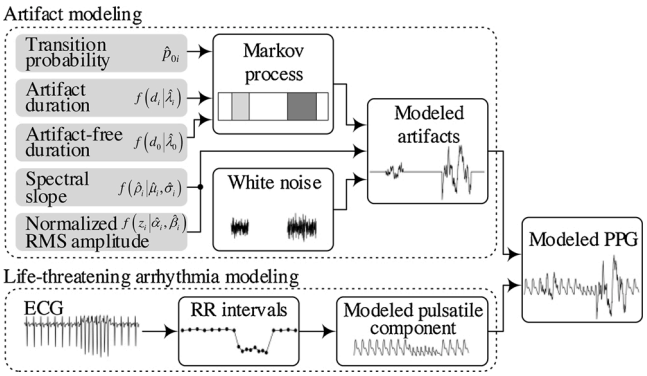

Fig. 3. Block diagram for modeling of the PPG signal with life-threatening arrhythmias and artifacts.

4. Databases

Three databases were used in this work. The standardized artifact database, created by performing artifact-inducing activities, was employed to determine the thresholds for artifact classification into four distinct types. The ambulatory database, collected at cardiac rehabilitation hospital, was used to analyze artifact characteristics. The ECG arrhythmia database served as a basis to simulate equivalent PPGs with life-threatening arrhythmia episodes and demonstrate the application of the artifact model to testing an arrhythmia detector.

4.1. Standardized artifact database

The standardized artifact database consists of signals from ten healthy participants (five females), with age 27.1 ± 2.3 years and body-mass index $22.3 \pm 2.5 \mathrm{kg/m^2}$, gathered at the Biomedical Engineering Institute (Kaunas, Lithuania) on a voluntary basis. The database was collected using a wrist-worn device capable of synchronously acquiring PPG (green light-emitting diode) and three-axis accelerometer signals, sampled at 100 Hz, and a single-lead ECG, sampled at 500 Hz [39]. The database was collected according to the following protocol in which the participants had to [23]:

1) remain still for 1 min with the properly attached wrist-worn device;
2) perform four different periodic hand motions (index finger tapping, fist opening and closing, radial and ulnar deviation, wrist extension and flexion) for 50 s with 10-s rest period in between;
3) perform three different periodic forearm motions (horizontal hand waving, vertical hand shaking, running arm swing) for 50 s with 10 s of rest in between and 50 s of intensive haphazard forearm motion with 10 s of rest;
4) move the device intentionally with the other hand for 1 min to imitate device displacement;
5) remain still for 1 min with the loosely attached device to imitate poor contact.

The periodic motions were performed at a frequency of 0.5 Hz using a metronome.

Twenty-five 2-s artifacts of each type were extracted for each participant resulting in a balanced dataset containing 1000 artifacts in total. To investigate the influence of the minimal artifact duration $d_{\min}$ on the classification performance, two additional datasets of 4-s and 6-s artifacts were also constructed. The classification performance was assessed by accuracy defined as the number of correctly identified artifacts divided by the total number of artifacts [40].

4.2. Ambulatory database

The ambulatory database was collected at Kulautuva Rehabilitation Hospital of Kaunas Clinics (Kaunas, Lithuania), with approval by the Kaunas Region Biomedical Research Ethics Committee (No. BE-2-20). Thirty-two patients (six females), 70.5 ± 9.4 years old, with body-mass index $28.0 \pm 5.2 \mathrm{kg/m^2}$, were enrolled. The total monitoring time was 686.1 h (21.4 ± 3.4 h per patient). The database was gathered during cardiac rehabilitation after myocardial infarction, thus the patients were physically active for several hours during the monitoring period, including participation in guided workout sessions.

4.3. Arrhythmia database

The developed PPG artifact model was applied to illustrate the influence of artifacts on the detection of life-threatening arrhythmias. ECGs from the PhysioNet/CinC Challenge 2015 database training set were used to simulate PPGs with extreme bradycardia and ventricular tachycardia [41]. Only those recordings with underlying sinus rhythm and the episodes of extreme bradycardia and ventricular tachycardia, with at least one ECG lead eligible for R-peak detection, were included. The subset consists of 16 recordings with extreme bradycardia and 39 with ventricular tachycardia, see Table 1.

The recordings of the database were originally reviewed by expert annotators who confirmed that each recording contains episodes of life-threatening arrhythmia without providing details on the onset and end. Therefore, the boundaries of arrhythmia episodes were manually identified according to the following rules: An episode was annotated as extreme bradycardia if heart rate dropped below 40 bpm for at least 5 consecutive beats, and as ventricular tachycardia if heart rate exceeded 120 bpm for at least 5 consecutive beats. Episodes were considered as individual if separated by at least 3 beats with no arrhythmia.

Taking into account that the duration of the PhysioNet/CinC Challenge 2015 recordings is only 5 min, which is too short to properly imitate arrhythmia detection in long-term recordings, the RR intervals were replicated and concatenated to form a 1-h-long RR interval series. By using the series as an input to the model described in [33,34], a 1-h pulsatile PPG component was generated and contaminated with artifacts of the desired properties. A Dawber's pulse Type 3 was chosen for simulating PPGs since it is a predominant pulse type among older individuals [38]. In total, the dataset consists of 227 episodes of extreme bradycardia with median length of 5 beats (ranging from 5 to 19) and 492 episodes of ventricular tachycardia with median length of 7 beats (ranging from 5 to 25).

The application of the artifact model to testing a life-threatening arrhythmia detector was demonstrated by implementing a basic threshold-based detector [14]. The same definitions of the life-threatening arrhythmias were invoked for the detection as described above. The detection performance was investigated in terms of sensitivity, defined as the number of correctly detected arrhythmia episodes divided by the total number of arrhythmia episodes, as well as, the number of false alarms per hour, and positive predictive value, defined as the number of correctly detected arrhythmia episodes divided by the

Table 1
The subset of the selected recordings from the PhysioNet/CinC Challenge 2015 database containing extreme bradycardia and ventricular tachycardia.

Extreme bradycardia		Ventricular tachycardia				
b220s	b515l	v131l	v309l	v632s	v733l	v803l
b227l	b516s	v132s	v368s	v635l	v748s	v806s
b228s	b517l	v206s	v369l	v648s	v758s	v815l
b229l	b656s	v253l	v404s	v696s	v769l	v818s
b265l	b764s	v254s	v471l	v701l	v772s	v828s
b299l	b794s	v255l	v574s	v714s	v773l	v831l
b455l	b838s	v275l	v628s	v726s	v788s	v837l
b456s	b839l	v290s	v630s	v729l	v797l	

total number of detected episodes.

5. Results

5.1. Parameter settings for artifact classification

Fig. 4 shows artifact classification accuracy as a function of threshold values. When the minimal artifact duration $d_{\min}$ is set to either 4 s or 6 s, similar classification accuracy is obtained, however, slightly better for 6 s. As a trade-off, 4-s minimal artifact duration is chosen to ensure that short artifacts are not overlooked. For $d_{\min} = 4$ s, the highest classification accuracy is obtained for the threshold values $\eta_u = 0.08$ g, $\eta_v = 11$ and $\eta_w = 0.015$. This threshold set yields the average classification accuracy of 0.98.

5.2. Artifact characteristics in the ambulatory database

Analysis of the ambulatory database shows that 26.8% of the total PPG duration is artifact-corrupted, covering from 13.6% to 48.6% depending on the recording (Fig. 5). Most of the artifacts were identified as device displacement, forearm motion, and hand motion, corrupting 6.4%, 6.2%, and 6.0%, whereas only 1.8% was assigned to poor contact. In addition, 6.4% of the PPG duration was flagged by the SQI as containing artifacts, but was not attributed to any type due to the artifact duration shorter than 4 s or unavailability of a good-quality reference ECG.

The percentage of the artifact-corrupted PPG within the day is given in Fig. 6. On average, at least a quarter of the PPG duration contains artifacts from 06:00 to 22:00 and drops markedly outside this period, which coincides well with the most active period of the day. Based on this finding, PPGs from the ambulatory database are subdivided to the periods of day- (06:00–22:00) and night-time (22:00–06:00). By using such subdivision, 37.0% of the total PPG duration is attributed to artifacts for day-time, and 8.8% for night-time.

The estimated transition probabilities from an artifact-free interval to each artifact type for day- and night-time periods are given in Table 2. The probabilities of having the device displacement and forearm motion artifacts are lower during night-time due to reduced movement, and vice versa during day-time.

Fig. 7 shows that the histograms of the duration of different-type artifacts and artifact-free intervals resemble an exponential distribution. Artifact-free intervals prolong during night-time as supported by the decreased rate parameter $\widehat{\lambda}_0$. This finding coincides with the fact that all types of artifacts are less frequent and usually shorter during night-time.

Fig. 8 presents the weighted average PSDs and the estimated slopes of different-type artifacts. The PSDs of hand motion and poor contact are apparently flatter because the spectral power is moved toward high frequencies, suggesting that artifacts are more noise-like.

The normalized RMS amplitude of different-type artifacts follows a

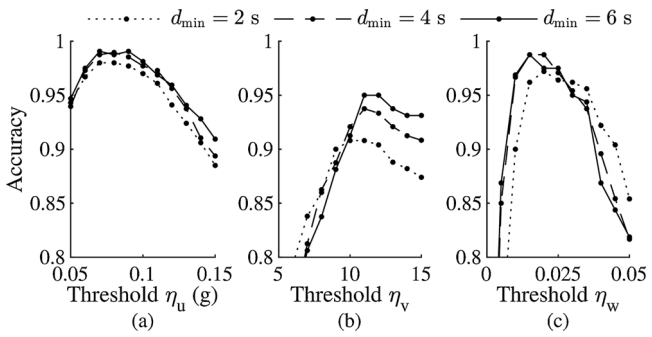

Fig. 4. Artifact classification accuracy as a function of a classification threshold for a different minimal artifact duration. (a) Classification accuracy between two groups of artifacts of which one group contains device displacement and forearm motion, and the other contains hand motion and poor contact. (b) Classification accuracy between device displacement and forearm motion. (c) Classification accuracy between hand motion and poor contact.

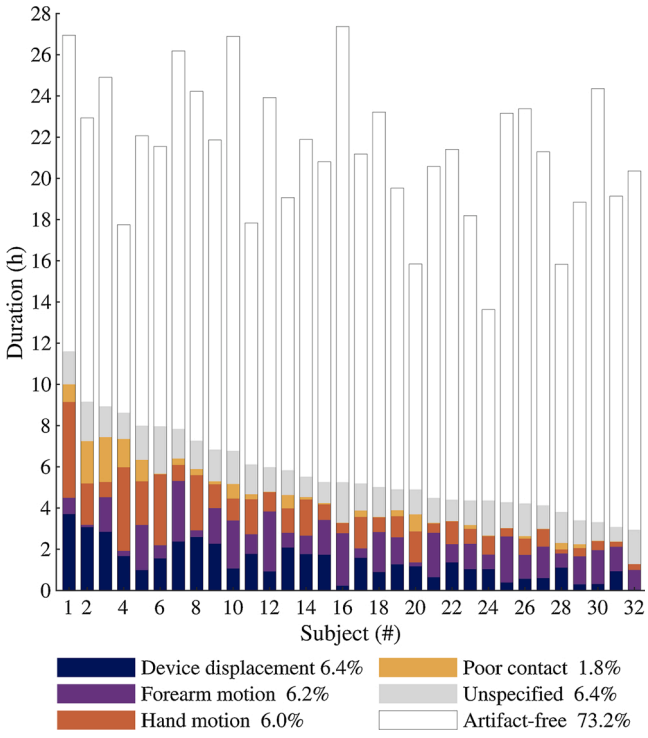

Fig. 5. Duration of different-type artifacts and artifact-free PPG intervals for all recordings of the ambulatory database. Data are sorted in descending order according to the total artifact duration.

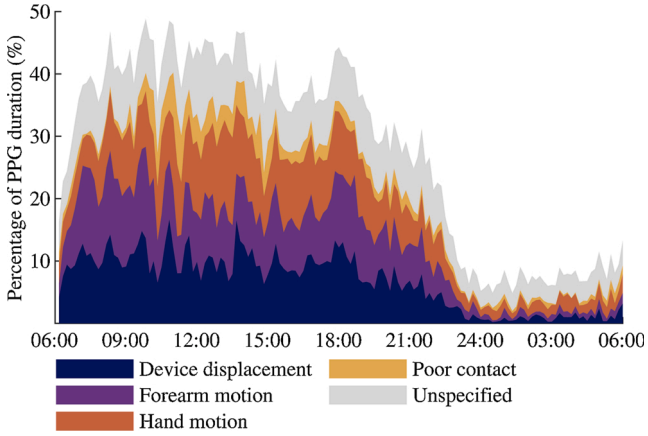

Fig. 6. Stacked diagram of the percentage of different-type artifacts occurring within the day. The artifact percentage is calculated in 10-min non-overlapping windows for the entire ambulatory database.

Table 2
Estimated transition probabilities from an artifact-free interval to a particular artifact type.

	Device displacement, $\widehat{p}_{01}$	Forearm motion, $\widehat{p}_{02}$	Hand motion, $\widehat{p}_{03}$	Poor contact, $\widehat{p}_{04}$
Day-time	0.23	0.37	0.31	0.09
Night-time	0.16	0.24	0.45	0.15

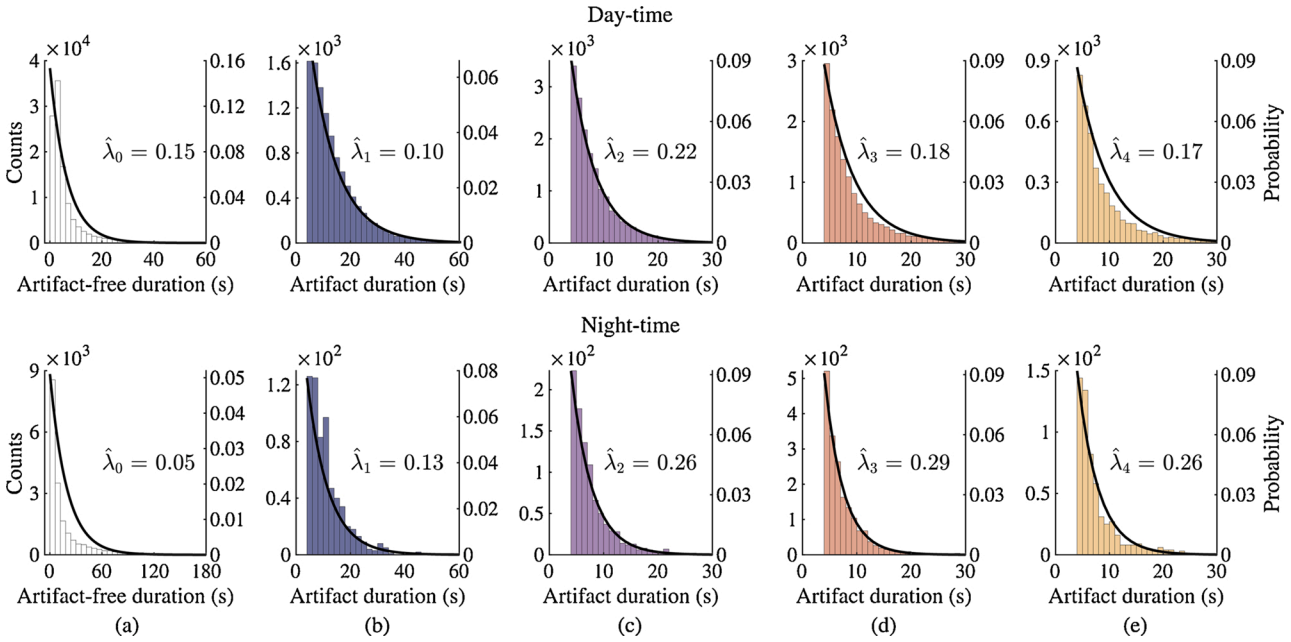

Fig. 7. Histograms of the day- and night-time duration of (a) artifact-free intervals, (b) device displacement, (c) forearm motion, (d) hand motion, and (e) poor contact artifacts. The histograms start at 4-s bin because of the chosen minimal artifact duration. Solid lines show the fitted exponential models with the estimated rate parameters $\hat{\lambda}_i$ given above.

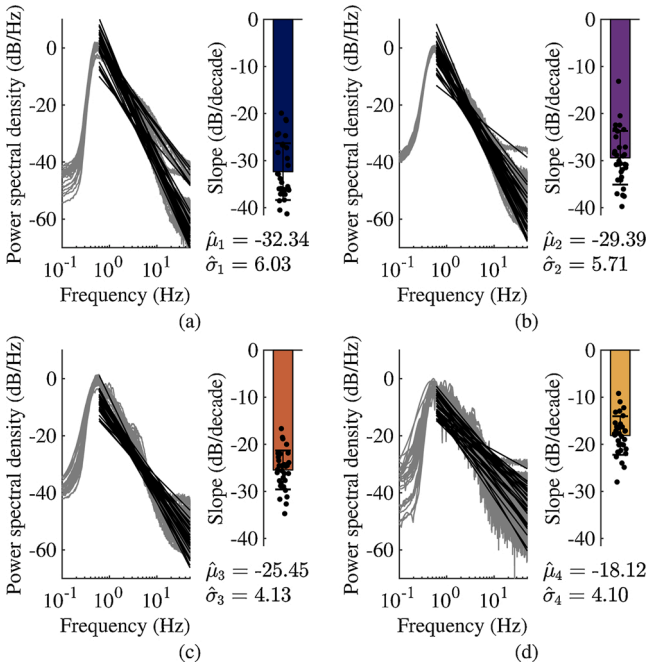

Fig. 8. Average PSDs and their estimated slopes of (a) device displacement, (b) forearm motion, (c) hand motion, and (d) poor contact artifacts for each recording of the ambulatory database. The PSDs up to 0.5 Hz are suppressed due to the removed slow-changing PPG component. Solid black line stands for the fitted PSD slope. Error bars show mean $\hat{\mu}_i \pm$ standard deviation $\hat{\sigma}_i$.

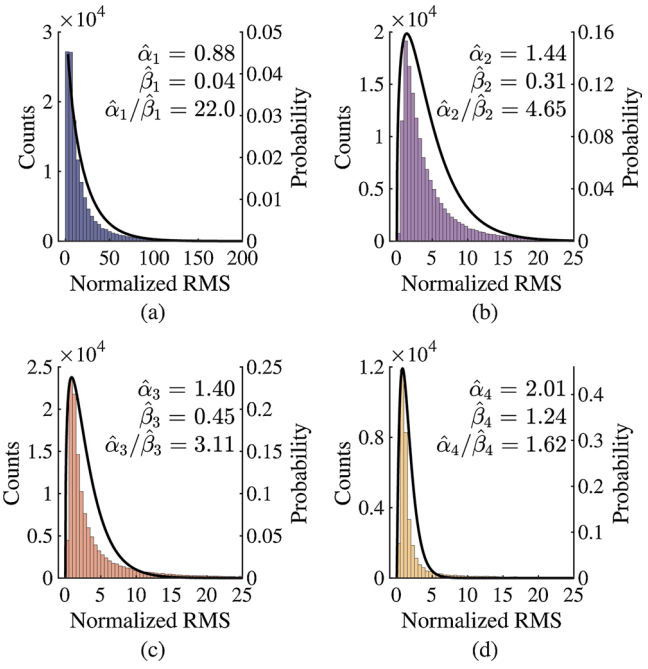

Fig. 9. Histograms of the normalized RMS amplitude in 1-s segments of (a) device displacement, (b) forearm motion, (c) hand motion, and (d) poor contact artifacts. The fitted gamma models are plotted as solid lines with the estimated shape $\hat{\alpha}_i$ and rate $\hat{\beta}_i$ parameters given above. The ratio $\hat{\alpha}_i/\hat{\beta}_i$ yields the mean of the distribution.

gamma distribution, see Fig. 9. Device displacement, on average, causes the largest artifact amplitude which is 22 times larger than that of the pulsatile PPG component. This proportion is considerably smaller for other artifact types.

5.3. *Testing of an arrhythmia detector*

Table 3 presents the arrhythmia detection performance for different types of artifacts. Irrespective of the artifact type, the sensitivity of extreme bradycardia detection drops nearly twice compared to the perfect sensitivity achieved for an artifact-free PPG. This can be explained by artifact-induced additional PPG pulses, which increase

Table 3
Performance of a life-threatening arrhythmia detector when a quarter of the PPG duration is contaminated with different types of artifacts.

	Artifact-free	Device displacement	Forearm motion	Hand motion	Poor contact	Mixture
Detection of extreme bradycardia						
Sensitivity	1.00	0.52	0.53	0.55	0.55	0.55
Positive predictive value	1.00	1.00	1.00	1.00	1.00	0.99
False alarms (1/h)	0.00	0.00	0.00	0.00	0.00	0.02
Detection of ventricular tachycardia						
Sensitivity	0.92	0.62	0.72	0.71	0.80	0.67
Positive predictive value	1.00	0.56	0.49	0.39	0.26	0.45
False alarms (1/h)	0.00	4.27	6.49	9.80	19.62	7.39

pulse rate and mask episodes of extreme bradycardia, but have less influence on the sensitivity of ventricular tachycardia detection. For the same reason, artifacts cause almost no false alarms of extreme bradycardia, resulting in nearly perfect positive predictive value, but adversely affect false alarm rate of ventricular tachycardia. Interestingly, poor contact causes 2–4 times more false alarms compared to the other artifact types. This can be explained by poor contact being the most difficult type to distinguish from the pulsatile PPG component.

Fig. 10 demonstrates the arrhythmia detection performance as a function of the percentage of the artifact-corrupted PPG, which is

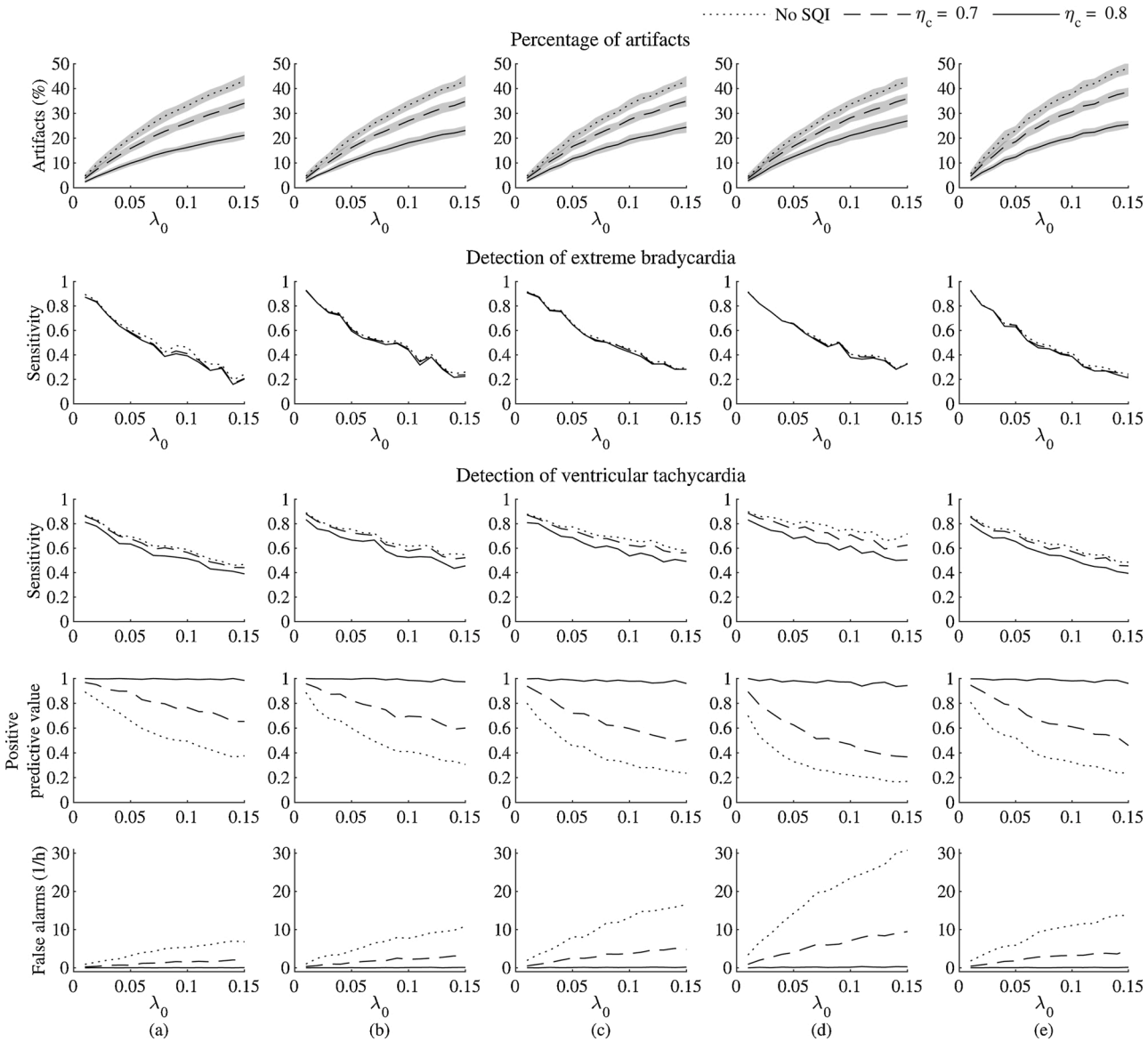

Fig. 10. The performance of life-threatening arrhythmia detection as a function of rate parameter λ_0 for different SQI threshold η_c. The functions are obtained for artifacts of (a) device displacement, (b) forearm motion, (c) hand motion, (d) poor contact, and (e) mixture of all artifact types. When only a single-type artifact is generated, the rate parameters determining the duration of each artifact are set to 0.2. For a mixture of all artifact types, the following estimated day-time values are used: $\widehat{\lambda}_1 = 0.10$, $\widehat{\lambda}_2 = 0.22$, $\widehat{\lambda}_3 = 0.18$ and $\widehat{\lambda}_4 = 0.17$. Shaded areas show mean ± standard deviation. Almost no false alarms are observed when detecting extreme bradycardia, and therefore positive predictive value is always close or equal to 1 (not shown).

governed by the rate parameter λ_0. By increasing λ_0 from 0.01 to 0.15, the average percentage of the artifact-corrupted PPG increased from 5% to 45%.

By applying the SQI, the amount of remaining artifacts is reduced with the expense of the duration of analyzable PPG. The use of the SQI has only a slight influence on the reduction in the detection sensitivity of both extreme bradycardia and ventricular tachycardia. However, the number of false alarms of ventricular tachycardia reduces markedly and the positive predictive value approaches 1. To nearly eliminate false alarms, a higher SQI threshold, e.g., $\eta_c = 0.8$, should be preferred, obviously at the expense of undetected arrhythmia episodes.

6. Discussion

The goal of this work is to develop a model for simulating artifacts in the wrist PPG. The PPG simulation model with realistic artifact component is of importance for developing and testing detectors for ambulatory arrhythmia monitoring. Albeit ECG will obviously remain a gold standard for arrhythmia detection, PPG-based devices show potential to become beneficial for prolonged monitoring of target populations and selection of individuals for comprehensive medical examination [7,8].

While the field of model application is definitely broader, this work focuses on the detection of life-threatening arrhythmias which often lead to sudden cardiac death. Such monitoring would be particularly valuable for end-stage kidney disease patients on hemodialysis who may experience life-threatening arrhythmias during the long interdialytic period when they are at home [42–45]. PPG-based detection of initial arrhythmia episodes could facilitate individual assessment of the risk–benefit ratio to guide decisions regarding cardiac device therapy, since hemodialysis patients are predisposed to post-implantation complications [46]. Another target population for the prolonged monitoring for the detection of life-threatening arrhythmias may be post-myocardial infarction patients who are at danger of sudden cardiac death during the first months after the event [47].

The proposed artifact model is developed by analyzing PPGs acquired during cardiac rehabilitation, thus provides insights into the quality of the wrist PPG encountered in free-living activities. In line with recent findings [48], our study shows that the percentage of the artifact-corrupted PPG markedly increases during day-time, mostly due to device displacement and forearm motion. This result supports a common observation that a substantial part of the day-time PPG is of insufficient quality for use in health monitoring applications [48].

In the ambulatory database, a quarter of the PPG duration was identified as corrupted by artifacts, which is higher than 10.8% reported in [10], but much lower than 44% in [12] and 65.2% in [48]. Possibly, the discrepancy between the studies arose from different conditions to acquire a PPG. Also, varying signal quality requirements, which often depend on the application, may have a substantial impact. Even slight PPG disturbance can be intolerable when PPG morphology is a subject to analysis, but may have a negligible effect on heart rate estimation. By applying a criterion of successful pulse detection, 42.4% of the total PPG duration was excluded in [13]. However, the percentage of unanalyzable PPG reached 76.0% by also accounting for the accelerometer-identified movement.

The identification of artifacts in the PPG depends on the chosen approach to PPG quality assessment. The most prevalent PPG artifacts are movement-related; therefore, a common practice is to involve an accelerometer for artifact identification [11–13,27–30]. Such approach may be ineffective in certain situations since artifacts may arise from other sources as well, e.g., poor contact and fine hand movements, which do not reflect in the accelerometer signals [23,27]. On the other hand, accelerometer-identified motion will not necessarily be a sign of the artifacts in the PPG. Relying solely on the accelerometer, a one-sixth of PPG pulses were falsely assigned to artifact-corrupted or artifact-free classes in the ambulatory database. That is, 8.3% of pulses were considered as artifact-free using the SQI, although flagged as artifacts by analyzing the accelerometer signals. Contrarily, 8.3% of artifact-corrupted pulses, identified by the SQI, were not reflected in the accelerometer signal. In the present study, pulse-to-pulse instead of a fixed-window SQI is preferred to achieve finer time resolution. Out of several pulse-to-pulse SQIs [10,49–51], only the one in [10] has been tested in long-term wrist PPGs acquired outside the laboratory setting and was therefore implemented in this study.

PPG artifacts have already been studied in a context of finger oximetry and neck photoplethysmography [52,53]. Nevertheless, these artifact characteristics cannot be straightforwardly transferred to simulating the wrist PPG since distinct body locations have different tissue optical properties for different wavelengths and are prone to specific interference [54]. In this study, artifact characteristics were obtained from a green-light PPG which is often used in commercial smartwatches to acquire pulse rate. Green is preferred to red and infrared since this wavelength does not penetrate deep into tissue causing fewer artifacts from a non-pulsatile slow-changing component [55]. In another study, the quality of a long-term green-light PPG, acquired using a smartwatch was investigated [48]. Yet, no artifact type-specific characteristics valuable for the model development were given.

The developed artifact model relies on the characteristics estimated from PPGs acquired during cardiac rehabilitation. Therefore, we assume that similar artifacts can be encountered in real-life PPGs. To ensure model flexibility, a transition probability from artifact-free interval to artifact, as well as an artifact duration, are free to be tuned to produce a desirable amount of artifacts. Such an approach excels other PPG simulators which generated stationary artifacts based on the characteristics of a single real artifact [33] or represented them as additive harmonic signals [56].

This study shows that the performance of the life-threatening arrhythmia detector is affected differently by different artifact types. Although device displacement substantially distorts the PPG, it is easily identified by the SQI due to the largest amplitude. On the other hand, poor contact disturbs the PPG so that additional pulses are produced making the identification of artifacts problematic. For this reason, additional pulses often lead to undetected extreme bradycardia, whereas have little effect on the detection of ventricular tachycardia.

The present study takes the first step toward investigating artifact influence on the detection of life-threatening arrhythmias in the PPG. Investigation of an atrial fibrillation detector showed that the specificity and the positive predictive value decrease with an increasing amount of artifacts [13]. The interesting finding of that study is the increase of the sensitivity proportional to the amount of the excluded artifact-corrupted PPG parts [13]. Our study shows contradictory results, i.e., the decrease in the sensitivity of ventricular tachycardia detection and no change in the sensitivity of extreme bradycardia detection for the increasing amount of the excluded PPGs. The contradiction arises since the sensitivity was calculated by including all arrhythmia episodes in our study, whereas only those episodes remaining after the exclusion of the artifact-corrupted PPG parts were included in [13]. This emphasizes the importance of using modeled PPGs to reveal the true detection performance taking into account arrhythmia episodes excluded together with poor-quality signals.

A limitation of the present study is that the developed model is restricted to simulating artifacts mostly caused by movement and device attachment. However, the intrinsic PPG disturbances originating from physiological processes, such as respiration, vasoconstriction due to temperature changes or stress [57], have not been considered.

7. Conclusions

The proposed PPG artifact simulation model is designed to facilitate the development and testing of wrist PPG-based arrhythmia detectors. Various artifact properties can be controlled by the model, including the

artifact type, the transition probabilities and the amount of artifact-corrupted PPG. Simulation of realistic artifacts encountered in activities of daily living allows to comprehensively investigate arrhythmia detectors and understand artifact types most negatively affecting detection performance.

Author contributions

Birutė Paliakaitė: conceptualization, methodology, software, validation, formal analysis, data curation, writing – original draft, visualization. Andrius Petrėnas: conceptualization, methodology, writing – review & editing. Andrius Sološenko: software, validation, writing – review & editing. Vaidotas Marozas: conceptualization, writing – review & editing, supervision, funding acquisition.

Data availability

The databases used in the current study are available from the corresponding author on request.

Funding

This work has received funding from European Regional Development Fund (Project No. 01.2.2-LMT-K-718-01-0030) under grant agreement with the Research Council of Lithuania (LMTLT).

Declaration of competing interest

The authors declare no conflict of interest.

References

[1] M. Hayashi, W. Shimizu, C.M. Albert, The spectrum of epidemiology underlying sudden cardiac death, Circ. Res. 116 (2015) 1887–1906, https://doi.org/10.1161/CIRCRESAHA.116.304521.

[2] K.-C. Yang, J.W. Kyle, J.C. Makielski, S.C. Dudley, Mechanisms of sudden cardiac death, Circ. Res. 116 (2015) 1937–1955, https://doi.org/10.1161/CIRCRESAHA.116.304691.

[3] M.C. Wong, J.M. Kalman, E. Pedagogos, N. Toussaint, J.K. Vohra, P.B. Sparks, P. Sanders, P.M. Kistler, K. Halloran, G. Lee, S.A. Joseph, J.B. Morton, Bradycardia and asystole is the predominant mechanism of sudden cardiac death in patients with chronic kidney disease, J. Am. Coll. Cardiol. 65 (2015) 1263–1265, https://doi.org/10.1016/j.jacc.2014.12.049.

[4] F.M. Kusumoto, K.R. Bailey, A.S. Chaouki, A.J. Deshmukh, S. Gautam, R.J. Kim, D. B. Kramer, L.K. Lambrakos, N.H. Nasser, D. Sorajja, Systematic review for the 2017 AHA/ACC/HRS guideline for management of patients with ventricular arrhythmias and the prevention of sudden cardiac death: a report of the American College of Cardiology/American Heart Association Task Force on Clinical Practice Guidelines and the Heart Rhythm Society, J. Am. Coll. Cardiol. 72 (2018) 1653–1676, https://doi.org/10.1016/j.jacc.2017.10.052.

[5] M.P. Turakhia, D.D. Hoang, P. Zimetbaum, J.D. Miller, V.F. Froelicher, U. N. Kumar, X. Xu, F. Yang, P.A. Heidenreich, Diagnostic utility of a novel leadless arrhythmia monitoring device, Am. J. Cardiol. 112 (2013) 520–524, https://doi.org/10.1016/j.amjcard.2013.04.017.

[6] S.R. Heckbert, T.R. Austin, P.N. Jensen, J.S. Floyd, B.M. Psaty, E.Z. Soliman, R. A. Kronmal, Yield and consistency of arrhythmia detection with patch electrocardiographic monitoring: the Multi-Ethnic Study of Atherosclerosis, J. Electrocardiol. 51 (2018) 997–1002, https://doi.org/10.1016/j.jelectrocard.2018.07.027.

[7] J.C. Nielsen, Y.-J. Lin, M.J. de Oliveira Figueiredo, A. Sepehri Shamloo, A. Alfie, S. Boveda, N. Dagres, D. Di Toro, L.L. Eckhardt, K. Ellenbogen, C. Hardy, T. Ikeda, A. Jaswal, E. Kaufman, A. Krahn, K. Kusano, V. Kutyifa, H.S. Lim, G.Y.H. Lip, S. Nava-Townsend, H.-N. Pak, G. Rodriguez Diez, W. Sauer, A. Saxena, J. H. Svendsen, D. Vanegas, M. Vaseghi, A. Wilde, T.J. Bunch, E.S.D. Group, A. E. Buxton, G. Calvimontes, T.-F. Chao, L. Eckardt, H. Estner, A.M. Gillis, R. Isa, J. Kautzner, P. Maury, J.D. Moss, G.-B. Nam, B. Olshansky, L.F. Pava Molano, M. Pimentel, M. Prabhu, W.S. Tzou, P. Sommer, J. Swampillai, A. Vidal, T. Deneke, G. Hindricks, C. Leclercq, European Heart Rhythm Association (EHRA)/Heart Rhythm Society (HRS)/Asia Pacific Heart Rhythm Society (APHRS)/Latin American Heart Rhythm Society (LAHRS) expert consensus on risk assessment in cardiac arrhythmias: use the right tool for the right outcome, in the right population, EP Europace 22 (2020) 1147–1148, https://doi.org/10.1093/europace/euaa065.

[8] C.C. Cheung, A.D. Krahn, J.G. Andrade, The emerging role of wearable technologies in detection of arrhythmia, Can. J. Cardiol. 34 (2018) 1083–1087, https://doi.org/10.1016/j.cjca.2018.05.003.

[9] G.H. Tison, J.M. Sanchez, B. Ballinger, A. Singh, J.E. Olgin, M.J. Pletcher, E. Vittinghoff, E.S. Lee, S.M. Fan, R.A. Gladstone, C. Mikell, N. Sohoni, J. Hsieh, G. M. Marcus, Passive detection of atrial fibrillation using a commercially available smartwatch, JAMA Cardiol. 3 (2018) 409–416, https://doi.org/10.1001/jamacardio.2018.0136.

[10] A. Sološenko, A. Petrėnas, B. Paliakaitė, L. Sörnmo, V. Marozas, Detection of atrial fibrillation using a wrist-worn device, Physiol. Meas. 40 (2019) 025003, https://doi.org/10.1088/1361-6579/ab029c.

[11] M.V. Perez, K.W. Mahaffey, H. Hedlin, J.S. Rumsfeld, A. Garcia, T. Ferris, V. Balasubramanian, A.M. Russo, A. Rajmane, L. Cheung, G. Hung, J. Lee, P. Kowey, N. Talati, D. Nag, S.E. Gummidipundi, A. Beatty, M.T. Hills, S. Desai, C. B. Granger, M. Desai, M.P. Turakhia, Large-scale assessment of a smartwatch to identify atrial fibrillation, N. Engl. J. Med. 381 (2019) 1909–1917, https://doi.org/10.1056/NEJMoa1901183.

[12] A.G. Bonomi, F. Schipper, L.M. Eerikäinen, J. Margarito, R. van Dinther, G. Muesch, H.M. de Morree, R.M. Aarts, S. Babaeizadeh, D.D. McManus, L. R. Dekker, Atrial fibrillation detection using a novel cardiac ambulatory monitor based on photo-plethysmography at the wrist, J. Am. Heart Assoc. 7 (2018) e009351, https://doi.org/10.1161/JAHA.118.009351.

[13] L.M. Eerikäinen, A.G. Bonomi, F. Schipper, L.R.C. Dekker, R. Vullings, H.M. de Morree, R.M. Aarts, Comparison between electrocardiogram- and photoplethysmogram-derived features for atrial fibrillation detection in free-living conditions, Physiol. Meas. 39 (2018) 084001, https://doi.org/10.1088/1361-6579/aad2c0.

[14] A.G. Bonomi, L.M. Eerikäinen, F. Schipper, R.M. Aarts, H.M. de Morree, L. Dekker, Detecting episodes of brady- and tachycardia using photo-plethysmography at the wrist in free-living conditions, Proc. Comput. Cardiol. Conf., vol. 44 (2017) 1–4, https://doi.org/10.22489/CinC.2017.271-329.

[15] Z. Zhang, Z. Pi, B. Liu, TROIKA: a general framework for heart rate monitoring using wrist-type photoplethysmographic signals during intensive physical exercise, IEEE Trans. Biomed. Eng. 62 (2015) 522–531, https://doi.org/10.1109/TBME.2014.2359372.

[16] E. Khan, F. Al Hossain, S.Z. Uddin, S.K. Alam, M.K. Hasan, A robust heart rate monitoring scheme using photoplethysmographic signals corrupted by intense motion artifacts, IEEE Trans. Biomed. Eng. 63 (2016) 550–562, https://doi.org/10.1109/TBME.2015.2466075.

[17] S. Fallet, J.-M. Vesin, Robust heart rate estimation using wrist-type photoplethysmographic signals during physical exercise: an approach based on adaptive filtering, Physiol. Meas. 38 (2017) 155–170, https://doi.org/10.1088/1361-6579/aa506e.

[18] Y. Fujita, M. Hiromoto, T. Sato, PARHELIA: particle filter-based heart rate estimation from photoplethysmographic signals during physical exercise, IEEE Trans. Biomed. Eng. 65 (2018) 189–198, https://doi.org/10.1109/TBME.2017.2697911.

[19] H. Chung, H. Lee, J. Lee, Finite state machine framework for instantaneous heart rate validation using wearable photoplethysmography during intensive exercise, IEEE J. Biomed. Health. Inf. 23 (2019) 1595–1606, https://doi.org/10.1109/JBHI.2018.2871177.

[20] A.J. Casson, A. Vazquez Galvez, D. Jarchi, Gyroscope vs. accelerometer measurements of motion from wrist PPG during physical exercise, ICT Express 2 (2016) 175–179, https://doi.org/10.1016/j.icte.2016.11.003.

[21] H. Lee, H. Chung, J. Lee, Motion artifact cancellation in wearable photoplethysmography using gyroscope, IEEE Sens. J. 19 (2019) 1166–1175, https://doi.org/10.1109/JSEN.2018.2879970.

[22] C. Zhou, J. Feng, J. Hu, X. Ye, Study of artifact-resistive technology based on a novel dual photoplethysmography method for wearable pulse rate monitors, J. Med. Syst. 40 (2015) 56, https://doi.org/10.1007/s10916-015-0412-2.

[23] Y. Zhang, S. Song, R. Vullings, D. Biswas, N. Sim oes-Capela, N. van Helleputte, C. van Hoof, W. Groenendaal, Motion artifact reduction for wrist-worn photoplethysmograph sensors based on different wavelengths, Sensors 19 (2019), https://doi.org/10.3390/s19030673.

[24] H. Lee, H. Chung, J. Kim, J. Lee, Motion artifact identification and removal from wearable reflectance photoplethysmography using piezoelectric transducer, IEEE Sens. J. 19 (2019) 3861–3870, https://doi.org/10.1109/JSEN.2019.2894640.

[25] J.D. Wander, D. Morris, A combined segmenting and non-segmenting approach to signal quality estimation for ambulatory photoplethysmography, Physiol. Meas. 35 (2014) 2543–2561, https://doi.org/10.1088/0967-3334/35/12/2543.

[26] B. Roy, R. Gupta, MoDTRAP: Improved heart rate tracking and preprocessing of motion-corrupted photoplethysmographic data for personalized healthcare, Biomed. Signal Process. Control 56 (2020) 101676, https://doi.org/10.1016/j.bspc.2019.101676.

[27] S.K. Bashar, D. Han, S. Hajeb-Mohammadalipour, E. Ding, C. Whitcomb, D. D. McManus, K.H. Chon, Atrial fibrillation detection from wrist photoplethysmography signals using smartwatches, Sci. Rep. 9 (2019) 15054, https://doi.org/10.1038/s41598-019-49092-2.

[28] M. Dörr, V. Nohturfft, N. Brasier, E. Bosshard, A. Djurdjevic, S. Gross, C.J. Raichle, M. Rhinisperger, R. Stöckli, J. Eckstein, The WATCH AF trial: SmartWATCHes for detection of atrial fibrillation, JACC Clin. Electrophysiol. 5 (2019) 199–208, https://doi.org/10.1016/j.jacep.2018.10.006.

[29] V.D.A. Corino, R. Laureanti, L. Ferranti, G. Scarpini, F. Lombardi, L.T. Mainardi, Detection of atrial fibrillation episodes using a wristband device, Physiol. Meas. 38 (2017) 787–799, https://doi.org/10.1088/1361-6579/aa5dd7.

[30] S. Fallet, M. Lemay, P. Renevey, C. Leupi, E. Pruvot, J.-M. Vesin, Can one detect atrial fibrillation using a wrist-type photoplethysmographic device? Med. Biol. Eng. Comput. 57 (2019) 477–487, https://doi.org/10.1007/s11517-018-1886-0.

[31] L.Y. Chen, M.K. Chung, L.A. Allen, M. Ezekowitz, K.L. Furie, P. McCabe, P. A. Noseworthy, M.V. Perez, M.P. Turakhia, Atrial fibrillation burden: moving beyond atrial fibrillation as a binary entity: a scientific statement from the American Heart Association, Circulation 137 (2018) e623–e644, https://doi.org/10.1161/CIR.0000000000000568.

[32] L.M. Eerikäinen, A.G. Bonomi, F. Schipper, L. Dekker, R. Vullings, H.M. de Morree, R.M. Aarts, How accurately can we detect atrial fibrillation using photoplethysmography data measured in daily life? Proc. Comput. Cardiol. Conf. (2019) 1–4, https://doi.org/10.23919/CinC49843.2019.9005802.

[33] A. Sološenko, A. Petrėnas, V. Marozas, L. Sörnmo, Modeling of the photoplethysmogram during atrial fibrillation, Comput. Biol. Med. 81 (2017) 130–138, https://doi.org/10.1016/j.compbiomed.2016.12.016.

[34] B. Paliakaitė, A. Petrėnas, A. Sološenko, V. Marozas, Photoplethysmogram modeling of extreme bradycardia and ventricular tachycardia, Proc. 15th Medit. Conf. Med. Biol. Eng. Comput. (2019) 1165–1174, https://doi.org/10.1007/978-3-030-31635-8_141.

[35] T. Wartzek, C. Brüser, T. Schlebusch, C. Brendle, S. Santos, A. Kerekes, K. Gerlach-Hahn, S. Weyer, K. Lunze, C. Hoog Antink, S. Leonhardt, Modeling of motion artifacts in contactless heart rate measurements, Proc. Comput. Cardiol. Conf., vol. 40 (2013) 931–934.

[36] F. Berief, S. Leonhardt, C. Hoog Antink, Modelling and synthesizing motion artifacts in unobtrusive multimodal sensing using copulas, Proc. Annu. Int. Conf. IEEE Eng. Med. Biol. Soc. (2018) 6006–6009, https://doi.org/10.1109/EMBC.2018.8513690.

[37] M. Aboy, J. McNames, D. Tran Thong, M.S. Tsunami, B. Ellenby, Goldstein, An automatic beat detection algorithm for pressure signals, IEEE Trans. Biomed. Eng. 52 (2005) 1662–1670, https://doi.org/10.1109/TBME.2005.855725.

[38] T.R. Dawber, H.E. Thomas, P.M. McNamara, Characteristics of the dicrotic notch of the arterial pulse wave in coronary heart disease, Angiology 24 (1973) 244–255, https://doi.org/10.1177/000331977302400407.

[39] D. Sokas, A. Petrėnas, S. Daukantas, A. Rapalis, B. Paliakaitė, V. Marozas, Estimation of heart rate recovery after stair climbing using a wrist-worn device, Sensors 19 (2019), https://doi.org/10.3390/s19092113.

[40] M. Sokolova, G. Lapalme, A systematic analysis of performance measures for classification tasks, Inf. Process. Manag. 45 (2009) 427–437, https://doi.org/10.1016/j.ipm.2009.03.002.

[41] A.L. Goldberger, L.A.N. Amaral, L. Glass, J.M. Hausdorff, P.C. Ivanov, R.G. Mark, J. E. Mietus, G.B. Moody, C.-K. Peng, H.E. Stanley, PhysioBank, PhysioToolkit, and PhysioNet: components of a new research resource for complex physiologic signals, Circulation 101 (2000) e215–e220, https://doi.org/10.1161/01.CIR.101.23.e215.

[42] P.A. Kalra, D. Green, D. Poulikakos, Arrhythmia in hemodialysis patients and its relation to sudden death, Kidney Int. 93 (2018) 781–783, https://doi.org/10.1016/j.kint.2017.12.005.

[43] S. Genovesi, G. Boriani, A. Covic, R.W.M. Vernooij, C. Combe, A. Burlacu, A. Davenport, M. Kanbay, D. Kirmizis, D. Schneditz, F. van der Sande, C. Basile, EUDIAL Working Group of ERA-EDTA, Sudden cardiac death in dialysis patients: different causes and management strategies, Nephrol. Dial. Transplant. (2019) 1–10, https://doi.org/10.1093/ndt/gfz182.

[44] P. Roy-Chaudhury, J.A. Tumlin, B.A. Koplan, A.I. Costea, V. Kher, D. Williamson, S. Pokhariyal, D.M. Charytan, on behalf of the MiD Investigators and Committees, Primary outcomes of the Monitoring in Dialysis Study indicate that clinically significant arrhythmias are common in hemodialysis patients and related to dialytic cycle, Kidney Int. 93 (2018) 941–951, https://doi.org/10.1016/j.kint.2017.11.019.

[45] M.C. Wong, J.M. Kalman, E. Pedagogos, N. Toussaint, J.K. Vohra, P.B. Sparks, P. Sanders, P.M. Kistler, K. Halloran, G. Lee, S.A. Joseph, J.B. Morton, Temporal distribution of arrhythmic events in chronic kidney disease: highest incidence in the long interdialytic period, Heart Rhythm 12 (2015) 2047–2055, https://doi.org/10.1016/j.hrthm.2015.06.033.

[46] G. Boriani, I. Savelieva, G.-A. Dan, J.C. Deharo, C. Ferro, C.W. Israel, D.A. Lane, G. La Manna, J. Morton, A.M. Mitjans, M.A. Vos, M.P. Turakhia, G.Y. Lip, ESC Scientific Document Group, Chronic kidney disease in patients with cardiac rhythm disturbances or implantable electrical devices: clinical significance and implications for decision making – a position paper of the European Heart Rhythm Association endorsed by the Heart Rhythm Society and the Asia Pacific Heart Rhythm Society, EP Europace 17 (2015) 1169–1196, https://doi.org/10.1093/europace/euv202.

[47] A.S. Adabag, T.M. Therneau, B.J. Gersh, S.A. Weston, V.L. Roger, Sudden death after myocardial infarction, JAMA 300 (2008) 2022–2029, https://doi.org/10.1001/jama.2008.553.

[48] N. Pradhan, S. Rajan, A. Adler, Evaluation of the signal quality of wrist-based photoplethysmography, Physiol. Meas. 40 (2019) 065008, https://doi.org/10.1088/1361-6579/ab225a.

[49] J.A. Sukor, S.J. Redmond, N.H. Lovell, Signal quality measures for pulse oximetry through waveform morphology analysis, Physiol. Meas. 32 (2011) 369–384, https://doi.org/10.1088/0967-3334/32/3/008.

[50] W. Karlen, K. Kobayashi, J.M. Ansermino, G.A. Dumont, Photoplethysmogram signal quality estimation using repeated gaussian filters and cross-correlation, Physiol. Meas. 33 (2012) 1617–1629, https://doi.org/10.1088/0967-3334/33/10/1617.

[51] P.K. Lim, S.-C. Ng, N.H. Lovell, Y.P. Yu, M.P. Tan, D. McCombie, E. Lim, S. J. Redmond, Adaptive template matching of photoplethysmogram pulses to detect motion artefact, Physiol. Meas. 39 (2018) 105005, https://doi.org/10.1088/1361-6579/aadf1e.

[52] M.T. Petterson, V.L. Begnoche, J.M. Graybeal, The effect of motion on pulse oximetry and its clinical significance, Anesth. Analg. 105 (2007) S78–84, https://doi.org/10.1213/01.ane.0000278134.47777.a5.

[53] I. García-López, E. Rodriguez-Villegas, Characterization of artifact signals in neck photoplethysmography, IEEE Trans. Biomed. Eng. (2020), https://doi.org/10.1109/TBME.2020.2972378, 1–1.

[54] Y. Maeda, M. Sekine, T. Tamura, Relationship between measurement site and motion artifacts in wearable reflected photoplethysmography, J. Med. Syst. 35 (2011) 969–976, https://doi.org/10.1007/s10916-010-9505-0.

[55] Y. Maeda, M. Sekine, T. Tamura, The advantages of wearable green reflected photoplethysmography, J. Med. Syst. 35 (2011) 829–834, https://doi.org/10.1007/s10916-010-9506-z.

[56] Q. Tang, Z. Chen, R. Ward, M. Elgendi, Synthetic photoplethysmogram generation using two Gaussian functions, Sci. Rep. 10 (2020), 13883, https://doi.org/10.1038/s41598-020-69076-x.

[57] J. Allen, Photoplethysmography and its application in clinical physiological measurement, Physiol. Meas. 28 (2007) R1–R39, https://doi.org/10.1088/0967-3334/28/3/r01.